Purdue University
Purdue e-Pubs

Birck and NCN Publications | Birck Nanotechnology Center

9-2010

Computational Study on the Performance of Si Nanowire pMOSFETs Based on the $k \cdot p$ Method

Mincheol Shin
Korea Advanced Institute of Science and Technology

Sunhee Lee
Purdue University - Main Campus

Gerhard Klimeck
Purdue University - Main Campus, gekco@purdue.edu

Follow this and additional works at: http://docs.lib.purdue.edu/nanopub

Part of the Nanoscience and Nanotechnology Commons

Shin, Mincheol; Lee, Sunhee; and Klimeck, Gerhard, "Computational Study on the Performance of Si Nanowire pMOSFETs Based on the k · p Method" (2010). *Birck and NCN Publications.* Paper 808.
http://dx.doi.org/10.1109/TED.2010.2052400

This document has been made available through Purdue e-Pubs, a service of the Purdue University Libraries. Please contact epubs@purdue.edu for additional information.

Computational Study on the Performance of Si Nanowire pMOSFETs Based on the $k \cdot p$ Method

Mincheol Shin, Sunhee Lee, and Gerhard Klimeck

***Abstract*—Full-quantum device simulations on p-type Si nanowire field-effect transistors based on the $k \cdot p$ method, using the $k \cdot p$ parameters tuned against the sp^3s^* tight-binding method, are carried out. Full transport calculations from both methods agree reasonably well, and the spin-orbit coupling effect is found to be negligible in the final current–voltage characteristics. Use of the highly efficient simulator based on the 3×3 $k \cdot p$ Hamiltonian is therefore justified, and simulations of nanowire devices with cross sections from 3×3 nm^2 up to 10×10 nm^2 are performed. The subthreshold characteristics, threshold voltages, and ON-state currents for the three respective transport directions of the [100], [110], and [111] directions are examined. The device characteristics for the [110] and [111] directions are quite similar in every respect, and the [100] direction has the advantage with regard to the subthreshold behavior when the channel length is aggressively scaled down. The ON-current magnitudes for the three respective orientations do not differ much, although the ON-current in the [100] direction is a little smaller, compared with that in the other two directions when the channel width becomes smaller. An uncoupled mode space approach has been used to determine the contributions from individual heavy and light hole subbands, enabling an insightful analysis of the device characteristics.**

***Index Terms*—Hole, $k \cdot p$, MOSFET, nanowire, nonequilibrium Green's function, PMOS, simulation, spin-orbit coupling, tight-binding, transistors, transport, valence band.**

I. Introduction

NANOWIRE field-effect transistors have recently attracted considerable attention as a possible next-generation candidate to replace the conventional planar metal–oxide semiconductor field-effect transistors, mainly due to their capability to enhance gate control to suppress short-channel effects [1]. N-type, as well as p-type, prototypes of such nanowire transistors with feature sizes of a few nanometers have been fabricated, and their device performance has been explored [2]–[4].

In this paper, we theoretically investigate the device performance limit of ideal p-type Si nanowire transistors (p-SNWTs) in the ballistic transport regime. There have been previous studies on the same issue, where the hole transport was semiclassically or full quantum-mechanically treated based on the tight-binding (TB) method [5]–[8]. In the semiclassical studies, the ON-state properties were examined [5]–[7] using the top-of-the-barrier (TOB) model [9], [10], but the subthreshold characteristics could not be addressed in short-channel devices [11], because quantum tunneling is disregarded in the TOB approach. The full quantum-mechanical study was rigorous in the treatment of hole transport; however, it was limited to ultranarrow nanowire devices due to the enormous computational burden, and only a few example calculations were performed [8].

This work uses a full-quantum device simulator based on the $k \cdot p$ method [12], [13]. The simulator is an order of magnitude or two faster than a full-quantum TB simulator and is capable of treating relatively thick nanowires, enabling us to perform a comprehensive and systematic examination of p-SNWTs as the nanowire thickness is gradually varied from 10 nm down to 3 nm.

The $k \cdot p$ method has widely been used to describe the valence band of Si [14]. It can also describe the coupling of heavy hole (HH) and light hole (LH) in confined systems, which results in warped subband structures. However, the $k \cdot p$ model is nonatomistic and needs to be benchmarked with respect to an atomistic model such as TB, which is regarded to be better suited for modeling nanowires with a-few-nanometer width. We carry out such benchmarking in this work and found out that the $k \cdot p$ and sp^3s^* TB methods agree reasonably well in terms of the final current–voltage characteristics. This could be expected, because fine differences arising from atomistic details should mostly disappear in a transport calculation where a few hundreds of millivolts are applied across the source and drain. However, it was not *a priori* clear if the two methods would agree in the description of transport in different wire directions with different atomic arrangements.

II. Approach

The approach to simulate the quantum transport in the p-SNWT shown in Fig. 1 is detailed in [12]. Here, we briefly outline the essential steps. We start with the 6×6 $k \cdot p$ Hamiltonian given by [14], [15]

$$H = \begin{bmatrix} H_{\rm int} & 0 \\ 0 & H_{\rm int} \end{bmatrix} + \Delta_{\rm so} \begin{bmatrix} iA & B \\ -B^* & -iA \end{bmatrix} \quad (1)$$

Manuscript received February 4, 2010; revised May 28, 2010; accepted May 28, 2010. Date of publication July 12, 2010; date of current version August 20, 2010. This work was supported in part by the Converging Research Center Program through the National Research Foundation of Korea funded by the Ministry of Education, Science and Technology, under Grant 2009-0094238; by the National Science Foundation (NSF) Grant EEC-0228390, which funds the Network for Computational Nanotechnology; by the NSF PetaApps Grant 0749140; by the Nanoelectronics Research Initiative through the Midwest Institute for Nanoelectronics Discovery, the Materials Structures and Devices Focus Center funded by the Focus Center Research Program; and by Sandia National Laboratory. The review of this paper was arranged by Editor M. Reed.

M. Shin is with the Department of Electrical Engineering, Korea Advanced Institute of Science and Technology, Daejeon 305-701, Korea (e-mail: mshin@kaist.ac.kr).

S. Lee and G. Klimeck are with the Network for Computational Nanotechnology, School of Electrical and Computer Engineering, Purdue University, West Lafayette, IN 47907-1285 USA.

Color versions of one or more of the figures in this paper are available online at http://ieeexplore.ieee.org.

Digital Object Identifier 10.1109/TED.2010.2052400

0018-9383/$26.00 © 2010 IEEE

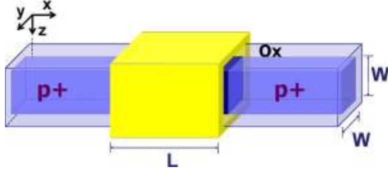

Fig. 1. Schematic diagram of the Si nanowire field-effect transistor considered in this work. L and W are the channel (gate) length and channel width, respectively.

where

$$H_{\text{int}} = \begin{bmatrix} \tilde{L}k_x^2 + Mk^2 & Nk_xk_y & Nk_xk_z \\ Nk_xk_y & \tilde{L}k_y^2 + Mk^2 & Nk_yk_z \\ Nk_xk_z & Nk_yk_z & \tilde{L}k_z^2 + Mk^2 \end{bmatrix} \quad (2)$$

is Kane's 3 × 3 interaction matrix that contains the parameters $\tilde{L} = -6\hbar^2\gamma_2/2m_0$, $M = -\hbar^2(\gamma_1 - 2\gamma_2)/2m_0$, and $N = -6\hbar^2\gamma_3/2m_0$, where γ_1, γ_2, and γ_3 are the Lüttinger parameters, Δ_{so} is the split-off parameter, and A and B are spin-orbit (SO) coupling matrices [15]. If SO is turned off, the Hamiltonian is reduced to H_{int} with double degeneracy. We next transform the $k \cdot p$ Hamiltonian H_K discretized in the k-space into the mode space via

$$H_M = U_M^{\dagger} H_K U_M \quad (3)$$

where U_M is the transformation matrix. To construct U_M, we first build a basis matrix U_0 whose mth column vector is the mth mode wavefunction, where modes are defined at $k = 0$ of the E–k diagram. We then diagonalize the matrix

$$h_i \equiv \epsilon_0 + U_0^{\dagger} V_i U_0 \quad (4)$$

where ϵ_0 represents the energies at the $k = 0$ of the E–k diagram, and V_i is the k-space 2-D potential profile of the ith cross section. If U_i is the unitary matrix that diagonalizes h_i in (4), we compute

$$U_M(i) = U_0 U_i. \quad (5)$$

The mode transformation matrix U_M in (3) is obtained by having $U_M(i)$ as its block diagonals. Lastly, the thus-constructed mode-space Hamiltonian H_M in (3) is fed into the recursive Green's function routine to calculate the hole density, which is, in turn, given to the 3-D Poisson's equation to produce an updated potential profile. These steps are repeated until self-consistency is achieved, and then, the drain current is calculated using the Landauer-Büttiker formula.

We note that the preceding mode-space transformation leads to a highly efficient simulation. The number of modes N_M that are needed to practically reproduce full solutions are usually 100 to 200, as has been verified in [12], and so, the size of the mode-space Hamiltonian, as well as the size of the cross-sectional eigenvalue problem in (4), is reduced to N_M.

III. BENCHMARKING

A. Determination of the $k \cdot p$ Parameters in Nanowires

The $k \cdot p$ parameters in the bulk Si are well established in the literature, but it is not known whether the same parameters can be continued to be used in nanowires. In this paper, we have determined the $k \cdot p$ parameters in nanowires by best matching the band structure by the $k \cdot p$ method to the band structure by the sp^3s^* TB method.

TABLE I
TUNED $k \cdot p$ PARAMETERS VERSUS NANOWIRE CROSS SECTIONS

Cross-section (nm^2)	γ_1	γ_2	γ_3	Δ_{so}
10x10	3.92	0.68	1.31	0.044
9x9	3.88	0.67	1.30	″
8x8	3.84	0.68	1.29	″
7x7	3.78	0.68	1.27	″
6x6	3.72	0.67	1.25	″
5x5	3.60	0.67	1.21	″
4x4	3.44	0.68	1.18	″
3x3	3.22	0.65	1.12	″

For the best matching, we have exhaustedly scanned the $k \cdot p$ parameter space for each nanowire cross section. The thus-obtained "tuned" $k \cdot p$ parameters are listed in Table I. A parameter set that best matches band structures in one direction (i.e., [100] direction) also best matches band structures in other directions (i.e., [110] or [111] directions). The same is true for SO; that is, the same parameter set best matches band structures whether SO is turned on or off. The $k \cdot p$ parameters in Table I show the pattern that γ_1 and γ_3 decrease but γ_2 stays almost the same as the nanowire cross section becomes smaller. This leads to effective masses of HH and LH that become heavier as the cross section becomes smaller, as will be discussed in more detail in later sections.

Fig. 2 illustrates an example of band-structure change before and after the tuning. Fig. 2(a) shows the band structure by the $k \cdot p$ method using the bulk parameters [16] ($\gamma_1 = 4.285$, $\gamma_2 = 0.339$, $\gamma_3 = 1.446$, and $\Delta_{\text{so}} = 0.044$). The band structure looks quite different from the band structure generated by the sp^3s^* TB method [Fig. 2(c)], and the quantization energies also differ by about 25 meV. Fig. 2(b) shows the band structure by the $k \cdot p$ method using the tuned parameters, which is much closer to the TB band structure.

B. Benchmarking With TB Full Transport Calculations

We have just shown that the band structure by the $k \cdot p$ method and the band structure by the TB method can be brought close to each other by adjusting the $k \cdot p$ parameters. We can thus expect that the full transport calculations by the two methods would agree reasonably well. This section demonstrates that this is indeed the case.

For the TB transport calculations, full-quantum and self-consistent calculations were performed by using the OMEN simulator [17] with the sp^3s^* orbitals (without SO coupling). The $k \cdot p$ transport calculations were also full-quantum and self-consistent ones, which were performed by using the three-band SO-off Hamiltonian, under the same conditions (such as the device dimensions and dopings) as the TB calculations. However, the location of the Si-oxide interface for the $k \cdot p$ calculations was adjusted by the distance equal to the Si atomic spacing (0.136 nm for [100] direction, for instance) to better match $k \cdot p$ and TB calculations. This modification is motivated by the fact that the location of the Si-oxide interface cannot exactly be

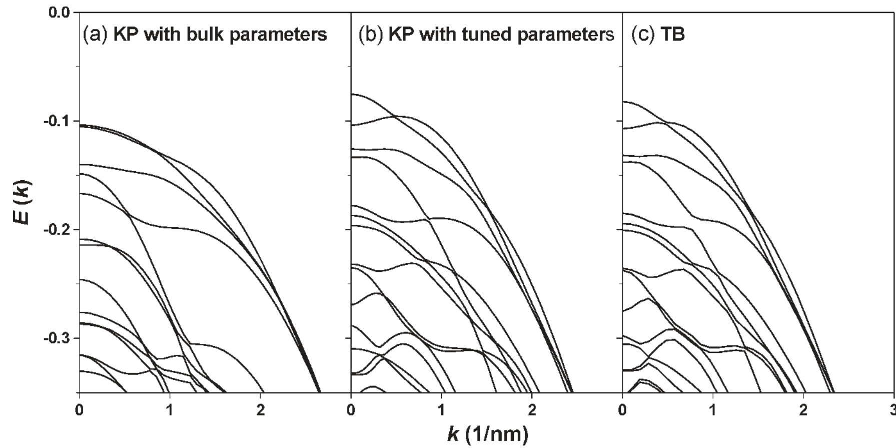

Fig. 2. Band structures of the Si [100] nanowire with 5×5 nm^2 cross section by (a) the $k \cdot p$ method using the bulk parameters, (b) the $k \cdot p$ method using the tuned parameters, and (c) the sp^3s^* TB method. The band structures by the $k \cdot p$ method were generated by constructing the k-space Hamiltonian, as detailed in [12], rather than a real-space Hamiltonian that depends on the spatial node resolution.

mapped between atomic positions (TB) and continuum meshes ($k \cdot p$), and thus, it is uncertain within one atomic spacing.

Fig. 3 shows the results of the two methods. The devices with 5×5 nm^2 cross section and 10-nm length and the devices with 3×3 nm^2 cross section and 6-nm length are considered. The I–V curves based on the $k \cdot p$ and TB methods agree reasonably well, for all the three considered transport directions. (For each device shown in the figure, the gate work function for the TB calculation was adjusted, so that the I–V's from the two methods have the same $I_{\text{off}} = 10^{-8}$ A.) Although not shown here, we have observed a similar agreement for devices with different lengths (3 nm for the 3×3 nm^2 cross section and 5 nm for the 5×5 nm^2 cross section).

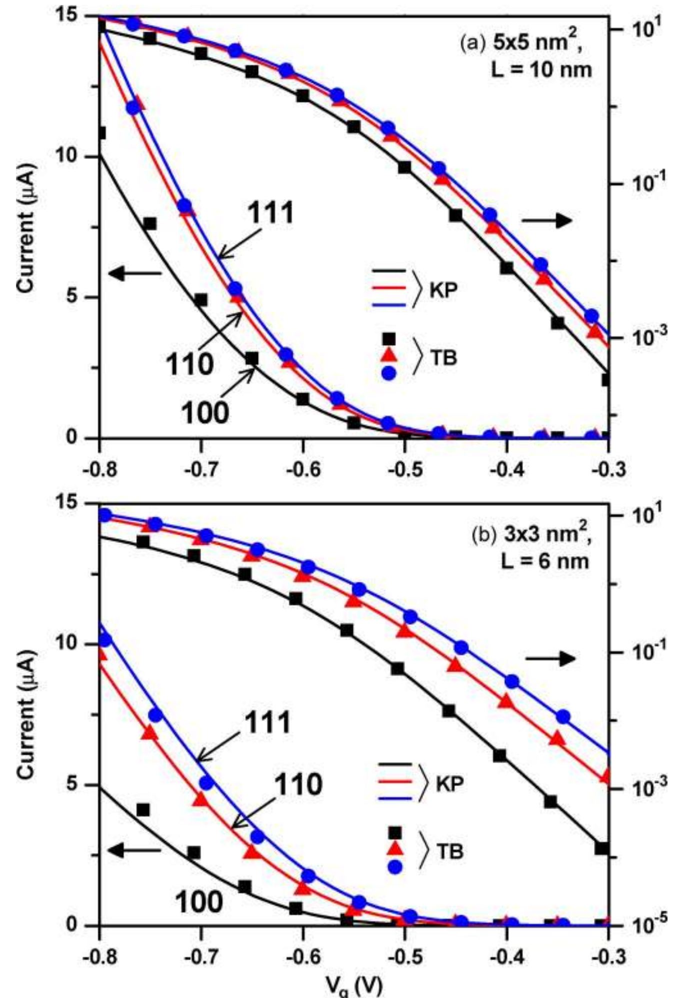

Fig. 3. Current–voltage characteristics calculated by using $k \cdot p$ and TB are compared for Si nanowires of (a) 5×5 nm^2 cross section and 10-nm channel length and (b) 3×3 nm^2 cross section and 6-nm channel length. Lines represent $k \cdot p$ results: black, red, and blue lines represent the [100], [110], and [111] directions, respectively. Symbols represent TB results: the solid squares, triangles, and circles represent the [100], [110], and [111] directions, respectively. The curves are plotted on both (left axis) a linear scale and (right axis) a log scale.

C. Effect of SO Coupling

As the Si nanowire size becomes smaller, the effect of SO coupling becomes more noticeable in the subband diagrams. However, our self-consistent calculations using the $k \cdot p$ parameters in Table I show that the effect of SO coupling is almost negligible in the final I–V characteristics, as can be seen in Fig. 4: in the devices with 5×5 nm^2 cross section and 5-nm length and the devices with 3×3 nm^2 cross section and 12-nm length, the calculations with SO and without SO yield almost overlapping I–V curves for each of the three considered transport directions. Although not shown, we have verified that the same is true for devices with different lengths (3 and 6 nm for 3×3 nm^2 cross section and 10 and 20 nm for 5×5 nm^2 cross section).

D. Uncoupled Mode Approach as an Analysis Tool

From the coupled mode-space approach previously described, it is hard to figure out how much each subband contributes to the total current. We introduce the uncoupled mode (UM) model in this work as an analysis tool to know that information.

In our UM model, modes are independent and uncoupled from other modes. Its implementation is straightforward: a

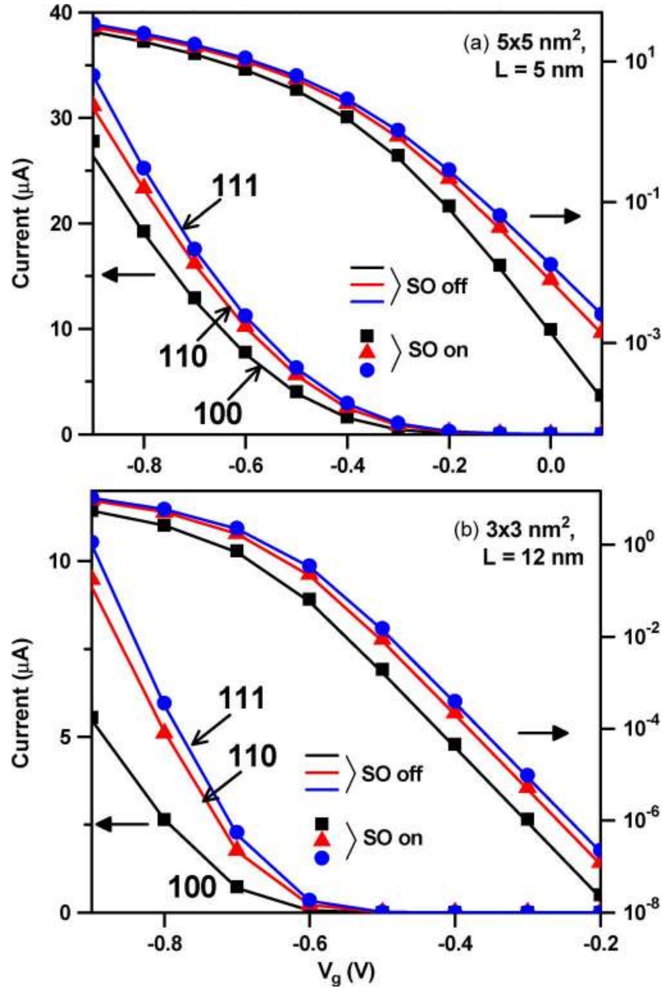

Fig. 4. Current–voltage characteristics calculated by using the 3 × 3 (SO-off) and 6 × 6 (SO-on) $k \cdot p$ methods are compared for Si nanowires of (a) 5 × 5 nm^2 cross section and 5-nm channel length and (b) 3 × 3 nm^2 cross section and 12-nm channel length. Lines represent SO-off results: black, red, and blue lines represent the [100], [110], and [111] directions, respectively. Symbols represent SO-on results: the solid squares, triangles, and circles represent the [100], [110], and [111] directions, respectively.

single-mode Hamiltonian for each independent mode is constructed, and its charge density and currents are calculated using the same routine, as described in Section II. The total charge density and currents are obtained by simply summing over contributions from individual modes. Modes are coupled only through the total charge density in the Poisson's equation.

A subband structure for a Si nanowire with 5 × 5 nm^2 cross section generated by the UM model is shown in Fig. 5(a). A flat constant cross-sectional potential profile is assumed in generating the subband structure. As indicated in the figure, where the transport direction is along the [100] direction, two groups of subbands with different curvatures are present in the subband diagram from the UM model. The subbands with smaller (greater) curvature have the curvature effective mass, which is exactly the same as the bulk heavy (light) hole effective mass from the bulk $k \cdot p$ Hamiltonian, given by [18]

$$m_{\mathrm{hh,bulk}}(100) = \frac{1}{\gamma_1 - 2\gamma_2} \tag{6}$$

$$m_{\mathrm{lh,bulk}}(100) = \frac{1}{\gamma_1 + 4\gamma_2}. \tag{7}$$

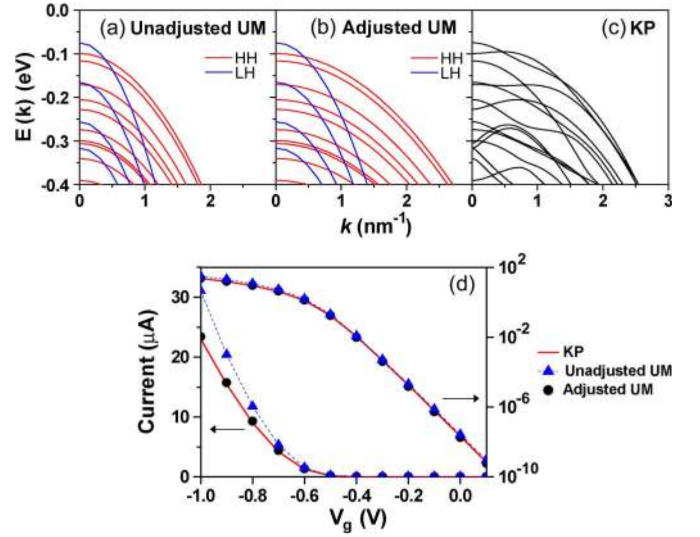

Fig. 5. Subband structures generated by using (a) the unadjusted UM, (b) the adjusted UM, and (c) the KP methods for the Si nanowire of 5 × 5 nm^2 cross section and 10-nm channel length. In (a) and (b), the LH and HH subbands are colored blue and red, respectively. The current–voltage characteristics for the three cases are compared in (d).

We therefore call the two groups of subbands HH and LH subbands, respectively. In the [110] direction, the HH and LH subbands can be similarly identified by using the UM model, although the HH subbands of the UM model have effective masses that are not exactly the same as the bulk effective mass from the bulk $k \cdot p$ Hamiltonian.

In the subband structure of the UM model in Fig. 5(a), the band warping due to coupling of holes is absent. As a consequence, the UM approach results in serious deviations from the full calculations in the current–voltage characteristics [see Fig. 5(d)]. This is in contrast to the case of electron transport in n-type devices, where it has been shown that the UM approach produces results sufficiently close to coupled-mode or real-space results [19].

The mode coupling, which is absent in our UM model, can be "effectively" taken into account by manually adjusting the curvature effective masses of the HH and LH subbands. For example, for the device considered in Fig. 5(a), the effective masses of the HH and LH subbands are adjusted from $0.44m_0$ and $0.16m_0$ to $0.92m_0$ and $0.23m_0$, respectively. Then, the subband structure from the "adjusted" UM model mimics the subband structure from the $k \cdot p$ method better, and more importantly, the current–voltage characteristics from the two can be brought close to each other (see Fig. 5). The current distribution as a function of energy also shows close similarity between the two, as will be shown later (see Figs. 8 and 14). Let us call the original coupled-mode $k \cdot p$ method the KP method and the adjusted uncoupled-mode $k \cdot p$ method the UM-KP method.

Since the subbands are independent in the UM-KP model, one can easily figure out how much each subband contributes to the transport. This separation of holes can provide significant insight. In this paper, we will extensively use the UM-KP model in examining the transport in the subthreshold region, as well as in the ON-state. We stress, however, that our UM-KP model is not intended to be the one that can perfectly replace the KP method. We also note that we have not attempted to apply our

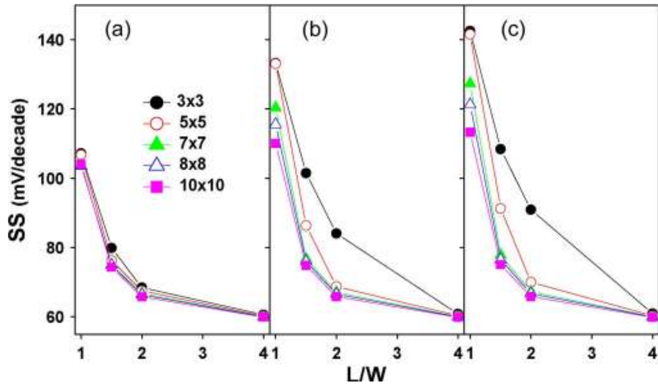

Fig. 6. SS versus L/W for the (a) [100], (b) [110], and (c) [111] directions for Si nanowires with (solid circle) 3 × 3, (open circle) 5 × 5, (solid triangle) 7 × 7, (open triangle) 8 × 8, and (solid square) 10 × 10 nm^2 cross sections.

UM model to the case of the [111] direction, because the device characteristics in the [110] and [111] directions are quite similar in every respect, as will be discussed shortly, and also because identification of the HH and LH subbands by using the UM model is ambiguous in this direction.

IV. Results and Discussion

The preceding results prove that the $k \cdot p$ simulator can produce results that are comparable with those of the TB simulator and that the effect of SO in full transport calculations is almost negligible. Based on the facts, we simulated the hole transport in p-SNWTs using our $k \cdot p$ simulator with the three-band SO-off $k \cdot p$ Hamiltonian with the tuned $k \cdot p$ parameters in Table I. The oxide thickness is assumed to be 1 nm, the source–drain doping is fixed at 10^{20} cm^{-3}, and all-around gates are used.

A. Tunneling Currents and Subthreshold Behavior

The effect of the channel length scaling down on the subthreshold behavior is examined first. Fig. 6 shows the dependence of the subthreshold slope (SS) on the channel length L for the [100], [110], and [111] transport directions, respectively, where the channel width W is varied from 10 to 3 nm. Note that the channel length is scaled by L/W in the figure. The SS values of the long-channel devices are close to the thermal limit of 60 mV/dec, irrespectively of the channel width and transport orientation. That implies that the tunneling-current contribution to the total current in the subthreshold region is small in the long-channel devices, which can be confirmed in Fig. 7.

As the channel length becomes shorter, the tunneling component in the total current is increased (Fig. 7), and the SS value increases accordingly (Fig. 6). More importantly, it is observed that the SS behavior becomes dependent on the wire direction. That is, SS versus L/W in the [100] direction does not change much with W, whereas that for the other two directions increases considerably as W is reduced. In the [100] direction, the SS is increased to 107 mV/dec when $L = W = 3$ nm, whereas, in the [110] direction, it is increased to 133 mV/dec for the same device dimensions.

To explain the SS behavior in the short-channel case, the current contribution from each subband is examined using the UM-KP method. Fig. 8 illustrates that the subthreshold current

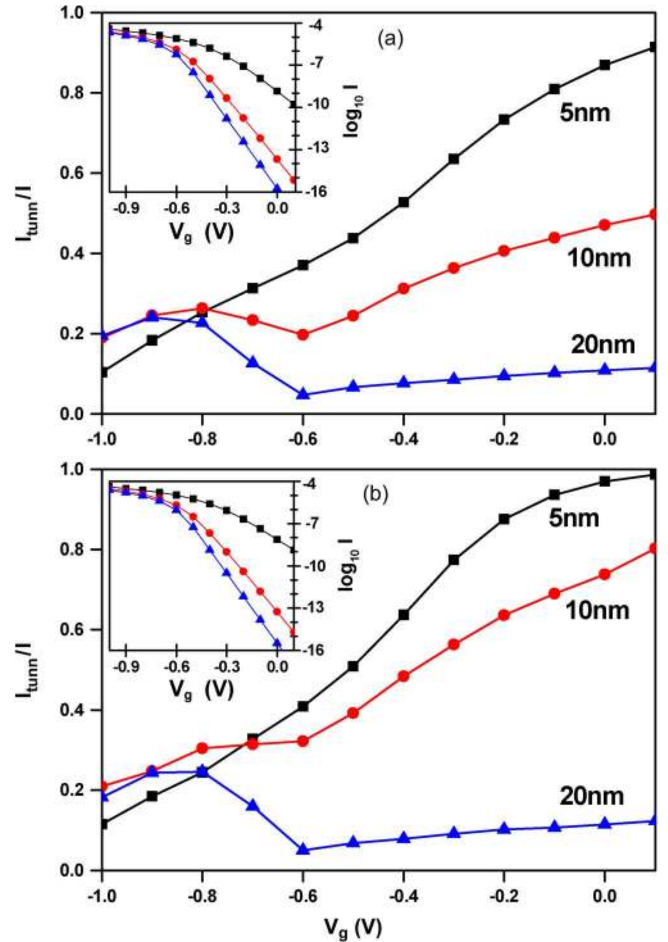

Fig. 7. Contribution of the tunneling current to the total current as a function of the gate voltage for p-SNWTs with 5 × 5 nm^2 cross section and (square) 5-nm, (circle) 10-nm, and (triangle) 20-nm channel length, respectively, in the (a) [100] and (b) [110] transport directions. Insets show the current–voltage characteristics of the corresponding devices.

in the short-channel case is dominated by the tunneling current from the topmost subband: in the figure, one can see that the current distributions from KP and UM-KP are in good agreement, which justifies the use of the UM-KP model, and that the top most subband dominantly contributes to the current. The topmost subband is of LH character, irrespective of the nanowire width and transport direction (see Figs. 5 and 14). Therefore, the SS of short-channel devices can be accounted for solely by the effective mass of the LH subbands of the UM-KP model.

Using the preceding findings, we have extracted the effective mass $m_{\rm lh}$ of the LH subbands through adjusting the effective mass, so that the SSs from KP and UM-KP agree with each other. Fig. 9 shows the dependence of $m_{\rm lh}$ on W. In both wire directions, $m_{\rm lh}$ becomes heavier with the decrease in W, but the increase rate is greater in the [100] direction. Fig. 10 shows that the increase in $m_{\rm lh}$ significantly suppresses otherwise faster increase in SS as W is decreased, and this effect is particularly more pronounced in the [100] direction, because $m_{\rm lh}$ increases faster in that direction. In the figure, $m_{\rm lh}$ is forced to be invariant to the decrease in W ($m_{\rm lh}$ at $W = 10$ nm is used), and the resultant SS is compared with the original SS. Notice

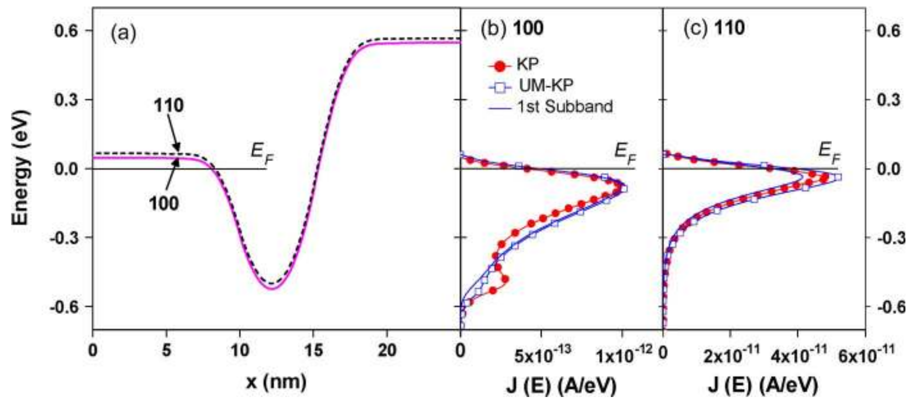

Fig. 8. (a) Example potential profiles in the OFF-state for the short-channel devices with 5 × 5 nm^2 cross section and 5-nm channel length. (b) Current distribution $J(E)$ with energy E for the [100] device in (a). Solid circles represent $J(E)$ calculated from KP and open squares from UM-KP. Solid lines with no symbols represent $J(E)$ from the first (topmost) subband. (c) The same for the [110] device in (a).

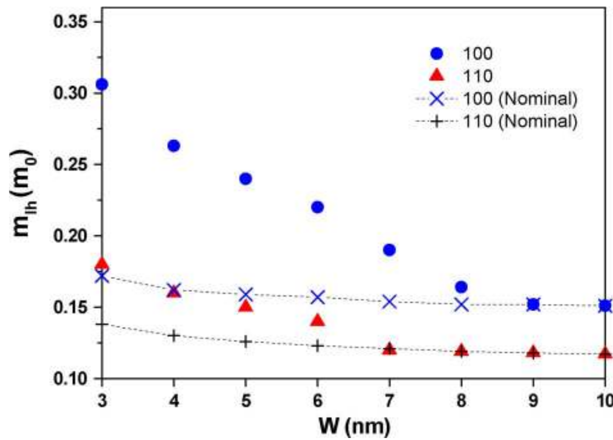

Fig. 9. $m_{\rm lh}$ as a function of nanowire width W in the [100] (circles) and [110] (triangles) directions. The nominal effective masses in the [100] (crosses) and [110] (pluses) directions are also shown.

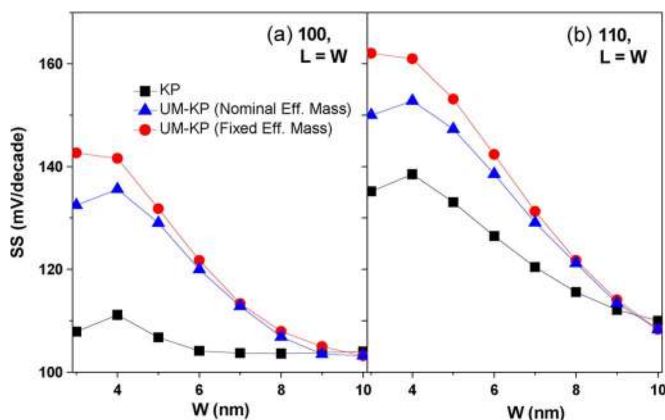

Fig. 10. Dependence of the SS of short-channel devices $(L/W = 1)$ on W for the (a) [100] and (b) [110] directions. Squares represent the SS from the KP method. Triangles represent the SS calculated from using the UM-KP approach, with the LH effective mass replaced by the nominal LH effective mass. Circles represent the SS calculated from using the UM-KP approach, with the LH effective mass fixed to and equal to the nominal LH effective mass for $W = 10$ nm.

in Fig. 10 that the SS of $L = W = 3$ nm is even slightly lower than that of $L = W = 4$ nm. This behavior is also supported by the TB calculation results.

The increase in the effective mass with the decrease in W is originated from two sources. The first one is the use of the $k \cdot p$ parameters in Table I, which gives rise to a slight increase in the "nominal" LH effective mass with respect to the decrease in W, as shown in Fig. 9. We define the nominal effective mass as the effective mass in the bulk from the 3×3 $k \cdot p$ theory, such as the ones given by (6) and (7). The nominal LH effective mass and $m_{\rm lh}$ of the UM-KP model are in good agreement for $W \geq$ 9 nm, but they become departed as W is reduced. The SS from using the UM-KP model with the LH effective mass replaced by the nominal LH effective mass is shown in Fig. 10: the slight increase in the nominal LH effective mass with decrease in W does not affect much the suppression of the increase in SS.

The second and more important source that brings about the increase in the effective mass with the decrease in W is the quantum-mechanical coupling of HH and LH. As the nanowire width becomes smaller, the coupling between holes becomes stronger due to the enhanced confinement effect. Our UM-KP model "effectively" captures the coupling effect, as previously mentioned, through the adjusted heavier effective mass. That is, the increase in $m_{\rm lh}$ reflects the fact that the coupling between holes is enhanced as W is decreased. In n-type nanowires, this kind of coupling between constituent charged particles does not exist, but TB results show that the electron effective mass is also seen to increase as the nanowire width becomes smaller [5]. This can be compared with the aforementioned increase in the nominal effective masses in p-type nanowires. (The nominal HH effective mass calculated using the $k \cdot p$ parameters in Table I also increases as W is decreased.)

We remark that, to the best of our knowledge, there has never been an attempt to separate LH and HH from the complicated subband structure in nanowires. A common practice, before our work, is that the topmost subband is fitted by a parabola and the extracted curvature effective mass $m_{\rm top}$ is used to explain the hole transport. Our result in this paper indicates that the common approach should not be adopted, because $m_{\rm top}$ can be *quite* different from $m_{\rm lh}$, especially in the [100] direction, where the coupling effect between holes is strong. $m_{\rm top}$ also increases—but only slightly—as W is reduced. Using the curvature effective mass $m_{\rm top}$, the different SS behavior by the transport direction cannot be explained.

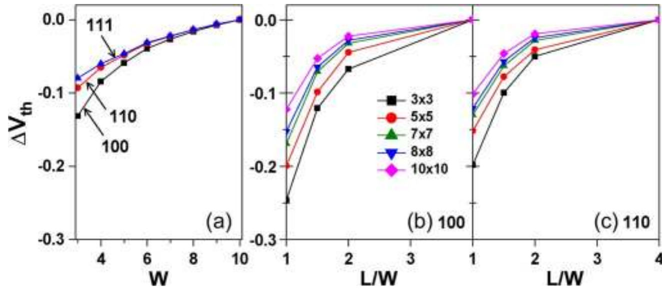

Fig. 11. (a) Threshold voltage change with respect to the decrease in W for the three respective directions. (b) and (c) Threshold voltage change with respect to L, as the nanowire cross section is varied as indicated. For each cross section, the threshold voltage change is obtained with reference to the device with the longest channel ($L/W = 4$).

We also remark that m_{hh}, which is the effective mass of the HH subbands of the UM-KP model, does not at all influence the subthreshold behavior. It was nevertheless extractable by adjusting the HH subband effective masses such that the I–V curves from the $k \cdot p$ and the UM methods are best matched in the *whole* gate-voltage range. (m_{lh} is usually fixed to the values obtained previously.) An example of such matching is shown in Fig. 5. However, we have found that the thus-obtained m_{hh} slightly depends on the nanowire channel length when the nanowire width is fixed, indicating the limitation of the UM-KP model. m_{hh} also shows a tendency to become heavier as W is decreased.

B. Threshold Voltage and DIBL

The threshold voltage change with respect to the nanowire channel width is shown in Fig. 11(a), where the threshold voltages were calculated in long-channel devices ($L/W = 4$). The threshold voltage change with W seems to be greater in the [100] direction, compared with the other two directions. A similar tendency was experimentally observed and explained in terms of the quantization energy in nanowires [4].

Fig. 11 also shows the change in the threshold voltage ΔV_{th} due to the shortening of the channel length for different channel widths and transport orientations. For each channel width, ΔV_{th} is calculated with reference to the device with the longest channel ($L/W = 4$). As in the case of the n-type counterpart, the threshold voltage in p-SNWTs also decreases as the channel length is shortened, and the device with smaller channel width shows greater variation of the threshold voltage by the channel-length shortening. In terms of the transport direction, the threshold voltage varies similarly in all the three directions considered, although the variation in the [100] direction is slightly greater, compared with the other two directions. If we refer to ΔV_{th} of the n-type Si nanowire transistor (SNWT) [20, Fig. 6], we can see that both the n-type SNWT and p-SNWT exhibit similar threshold voltage changes in terms of their magnitudes as well.

The drain-induced barrier lowering (DIBL) for 5×5 nm^2 and 10×10 nm^2 devices is shown in Fig. 12. The DIBL for the three transport directions seems to behave quite similarly as the channel length is gradually shortened, although the DIBL for the [100] direction is slightly lower than that in the other two directions. The DIBL of the n-type SNWT of the same dimensions is also shown in the figure for comparison (the data are from [21, Fig. 3]); notice the similarity in the DIBL between n-type SNWT and p-SNWT.

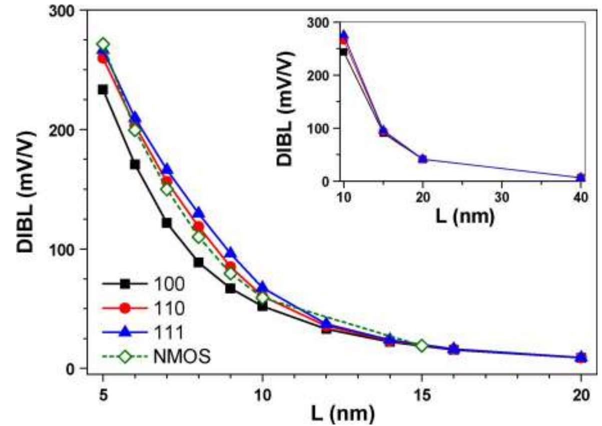

Fig. 12. DIBL as a function of L for p-SNWTs with 5×5 nm^2 cross section for the three respective directions indicated. The DIBL of [100] n-type SNWTs of the same dimensions is also shown for reference. (Inset) DIBL for p-SNWTs with 10×10 nm^2 cross section.

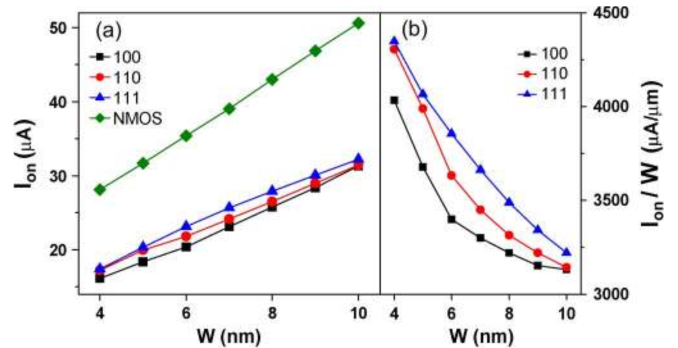

Fig. 13. (a) Dependence of the ON-currents of p-SNWTs on the nanowire width for the three respective directions indicated. The I_{on} of n-type SNWTs of the same dimensions are also shown for reference. (b) I_{on}/W of p-SNWTs versus W.

C. ON-Currents

Fig. 13 shows the ON-currents I_{on} of p-SNWTs in the three respective transport orientations, as the Si channel width is varied from 4 to 10 nm. (The ON-currents are calculated with $V_{\mathrm{DD}} = V_d = 0.5$ V after adjusting the gate work function, such that $I_{\mathrm{off}} = 10^{-8}$ A.) The difference in ON-currents by the transport orientation is observed to be quite small, which is particularly true for a larger width. At $W = 10$ nm, ON-currents differ by about 3%. As W becomes smaller, the difference tends to be larger, but it is about 15% at most. This result of ours is different from the result of the TB-TOB calculations in [6], where the ON-currents strongly depend on the nanowire orientation. (In the TB-TOB calculations, the semiclassical TOB model is used to calculate the ballistic current after the Si band structures from a TB Hamiltonian are obtained.)

Fig. 13 also shows the I_{on} of n-type SNWTs in the [100] direction as a comparison. The effective mass model is used to obtain the ON-currents of the n-type SNWTs. We observe that the I_{on} of p-SNWTs is about 50% of that of n-type SNWTs.

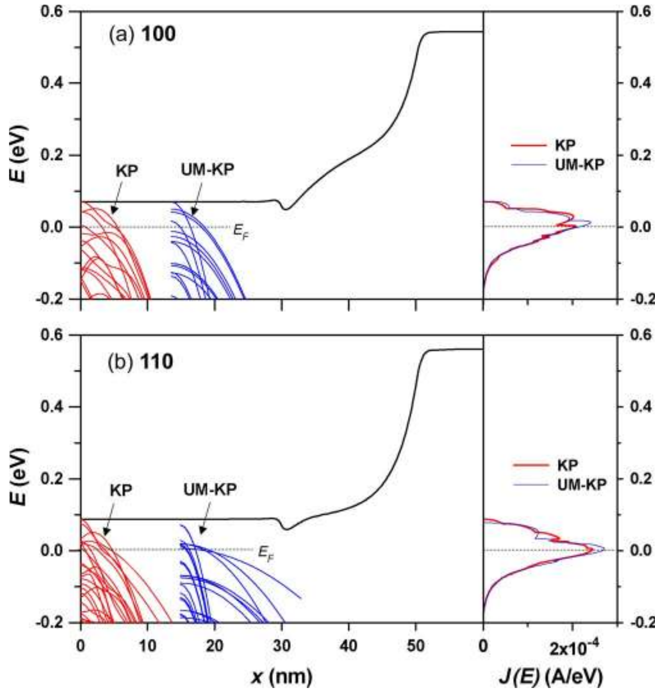

Fig. 14. Subband structures, potential profiles, and current distributions in the ON-state of p-SNWTs of 5×5 nm^2 cross section in the (a) [100] and (b) [110] transport directions. $J(E)$ from KP (thick red line) and that from UM-KP (thin blue line) are compared. The subband diagrams from full $k \cdot p$ (left, red color) and UM-KP (right, blue color) are also shown for reference.

A similar observation was made in [5], where the TB-TOB calculations were performed for [100] nanowires.

In the following, a detailed analysis on the ON-currents in p-SNWTs in the [100] and [110] orientations is performed. The behavior in the [111] direction is not explicitly discussed since it is similar to that in the [110] direction. Our main intention in this analysis is to figure out the contributions from the HH and LH to the total current. Fig. 14 shows the potential profiles, subband structures, and current distributions of [100] and [110] p-SNWTs in the ON-state, respectively, for the device with 5×5 nm^2 cross section. In the figure, the subband structures and current distributions obtained from the UM-KP model with the effective masses appropriately adjusted (see Fig. 5 for an example of such adjustment) are compared with those from the KP calculation. After confirming that the current distributions from KP and UM-KP agree with each other quite well, we are able to extract the contribution from each subband to the total current (see Fig. 15).

Fig. 15 shows that, first, there is not any single subband that dominantly contributes to the ON-current. Neither the topmost subband, which contributes about 25% to the overall current, nor the subbands near the Fermi energy can solely characterize the current behavior. In the figure, there are about ten subbands that contribute to the current. Second, more subbands are located around the Fermi energy in the [110] direction, compared with the [100] direction. Third, in the [100] direction, among the subbands that contribute to the current ($E \gtrsim -0.05$ eV), there are more HH subbands than LH subbands. The opposite is true for the [110] case. Specifically, in the [100] direction, the LH subbands together contribute about 45% of the total current, whereas, in the [110] direction, the total LH contribution is

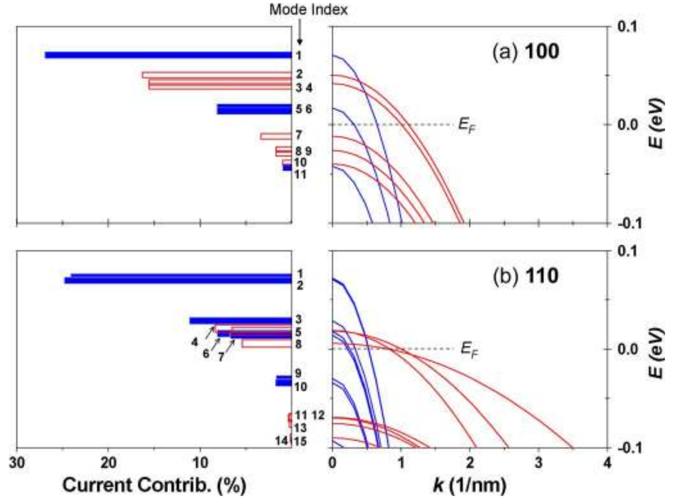

Fig. 15. Contribution by each subband to the total current (left panels) in the ON-state of p-SNWTs of 5×5 nm^2 cross section in the (a) [100] and (b) [110] transport directions. The corresponding subband diagrams from UM-KP (right panels) are also shown for reference. The bars of the left panels are positioned to the top of the corresponding subbands. The LH subbands and their contributions are colored and shaded blue, respectively. The HH subbands and their contributions are colored red.

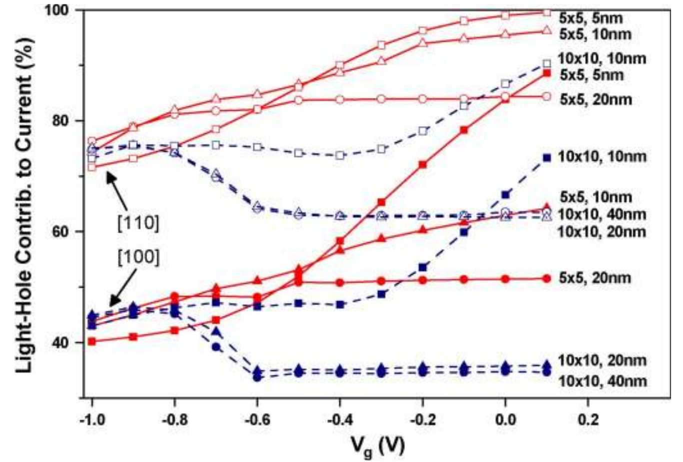

Fig. 16. Combined contribution from the LH subbands to the total current as a function of the gate voltage for p-SNWTs with various dimensions. Solid and dashed lines represent devices with 5×5 nm^2 and 10×10 nm^2 cross sections, respectively. Solid and open symbols represent devices in the [100] and [110] transport directions, respectively. Squares, triangles, and circles represent devices with the aspect ratio $L/W = 1$, 2, and 4, respectively.

about 75%. (The $m_{\rm lh}$ for the [100] and [110] directions are $0.23m_0$ and $0.15m_0$, respectively.) We have found that the same is true, regardless of the device dimensions, as discussed as follows:

Fig. 16 shows the ratio of the total LH current to the total current $r_{\rm lh} \equiv I_{\rm lh}/I$ as a function of the gate voltage. Devices with 5×5 nm^2 and 10×10 nm^2 cross sections and $L/W =$ 1, 2, and 4 are considered in the figure. $r_{\rm lh}$ in the [110] direction is overall higher than that in the [100] direction for the same nanowire dimensions. In the ON-state, $r_{\rm lh}$ approaches almost the same value, regardless of the nanowire dimensions, and around 0.45 and 0.75 for the [100] and [110] directions, respectively. For the short-channel case $(L/W = 1)$, $r_{\rm lh}$ in the OFF-state is close to 1 (or approaches 1 for negatively lower gate

voltages), which verifies our previous claim that the OFF-state current for short-channel devices is dominated by the current from the topmost subband, which is of LH character.

Let us now discuss the effective masses and their implication on the ON-currents in p-SNWTs. As can be seen in Fig. 15, the populations and locations of the LH subbands are different between the [100] and [110] directions, so the LH effective masses in the respective transport directions influence differently on the total on-currents. For instance, if $m_{\rm lh}$ in the [100] direction changes from $0.92m_0$ to $0.23m_0$, the total LH current $I_{\rm lh}$ and the total HH current $I_{\rm hh}$ are increased by 33% and 22%, respectively, and the overall ON-current is increased by 27%. On the other hand, if $m_{\rm lh}$ in the [110] direction is also reduced four times (from $0.60m_0$ to $0.15m_0$), both $I_{\rm lh}$ and $I_{\rm hh}$ are increased by 45%, and so, the overall ON-current is also increased by 45%. (Note that, if the effective masses of LH subbands are decreased, the Fermi energy is shifted away from the valence band top, and the tunneling probability of holes in the LH subbands becomes greater, leading to the increase in current from the LH subbands. The Fermi energy shift also leads to the increase in current from the HH subbands.) The aforementioned example calculation demonstrates that ON-current in p-SNWTs cannot be trivially scaled by the effective masses. In addition, as can be seen in Fig. 7, the tunneling-current contribution to the total current is not negligible, even in the ON-state. Therefore, any attempt to describe the ON-current with effective masses alone would poorly estimate it, e.g., the use of the concept of injection velocity with the injection velocity inversely proportional to the square root of some effective mass and without taking into account the tunneling probability.

We have previously mentioned that, overall, the difference in the ON-currents by the transport orientation is quite small. However, at a closer look, the difference between $I_{\rm on}(100)$ and $I_{\rm on}(110)$, in particular, grows as the nanowire width becomes smaller [see Fig. 13(b)]. The behavior can be explained in part by the fact that the LH effective mass depends on the nanowire width as in Fig. 9. As the nanowire width becomes smaller, $m_{\rm lh}(100)$ increases faster than $m_{\rm lh}(110)$, making the ON-current in the [100] direction smaller, compared with that in the [110] direction. We were able to verify using our UM-KP model that $I_{\rm on}(100)$ and $I_{\rm on}(110)$ stay closer if $m_{\rm lh}$ in the two directions changes at the same rate as W becomes smaller.

V. Conclusion

We have examined the device characteristics of p-type Si nanowire transistors based on the 3×3 $k \cdot p$ method after carefully justifying the use of the method. We have focused on the dependence of the device performance on the transport direction, as the nanowire channel size is gradually reduced from 10 to 3 nm in its width. Devices are assumed to be ideal, and the hole transport is ballistic in this study, but our work should give a guideline on the channel orientation effects in scaled nanowire devices.

We have found that the device characteristics are almost the same in the [110] and [111] directions, whereas the [100] direction shows a little different behavior. In terms of SS and DIBL, the [100] direction exhibits better performance with respect to the channel-length scaling-down. Especially, the [100] direction is preferable to the other two directions if SS is concerned, because the LH effective mass that becomes noticeably heavier as the nanowire width is decreased suppresses the tunneling current, which dominantly contributes to the subthreshold current.

In terms of the threshold voltage shift and ON-currents, on the other hand, the [100] direction turns out to be slightly unpreferable. However, the difference in ON-currents by the transport direction can be regarded to be quite small overall. A detailed analysis shows that the populations and locations of the HH and LH subbands are quite different by the transport direction: the light-hole subbands together contribute about 45% and 75% to the total ON-current for the [100] and [110] directions, respectively. We have also found that the ON-currents of p-type Si nanowire transistors are about half of the ON-currents of their n-type counterparts of the same dimensions.

Acknowledgment

The authors would like to thank D. Mathieu Luisier for the discussions.

References

[1] Y. Cui, Z. Zhong, D. Wang, W. Wang, and C. Lieber, “High performance silicon nanowire field effect transistors,” *Nano Lett.*, vol. 3, no. 2, pp. 149–152, 2003.

[2] N. Singh, F. Y. Lim, W. W. Fang, S. C. Rustagi, L. K. Bera, A. Agarwal, C. H. Tung, K. M. Hoe, S. R. Omampuliyur, D. Tripathi, A. O. Adeyeye1, G. Q. Lo, N. Balasubramanian, and D. L. Kwong, “Ultra-narrow silicon nanowire gate-all-around CMOS devices: Impact of diameter, channel-orientation and low temperature on device performance,” in *IEDM Tech. Dig.*, 2006, pp. 1–4.

[3] K. H. Cho, K. H. Yeo, Y. Y. Yeoh, S. D. Suk, M. Li, J. M. Lee, M.-S. Kim, D.-W. Kim, D. Park, B. H. Hong, Y. C. Jung, and S. W. Hwang, “Experimental evidence of ballistic transport in cylindrical gate-all-around twin silicon nanowire metal–oxide–semiconductor field-effect transistors,” *Appl. Phys. Lett.*, vol. 92, no. 5, pp. 052 102-1–052 102-3, 2008.

[4] M. Kobayashi and T. Hiramoto, “Experimental study on quantum confinement effects in silicon nanowire metal–oxide–semiconductor field-effect transistors and single-electron transistors,” *J. Appl. Phys.*, vol. 103, no. 5, pp. 053 709-1–053 709-6, 2008.

[5] J. Wang, A. Rahman, A. Ghosh, G. Klimeck, and M. Lundstrom, “Performance evaluation of ballistic silicon nanowire transistors with atomic-basis dispersion relations,” *Appl. Phys. Lett.*, vol. 86, no. 9, pp. 093 113-1–093 113-3, 2005.

[6] N. Neophytou, A. Paul, and G. Klimeck, “Bandstructure effects in silicon nanowire hole transport,” *IEEE Trans. Nanotechnol.*, vol. 7, no. 6, pp. 710–719, Nov. 2008.

[7] N. Neophytou and G. Klimeck, “Design space for low sensitivity to size variations in [110] PMOS nanowire devices: The implications of anisotropy in the quantization mass,” *Nano Lett.*, vol. 9, no. 2, pp. 623–630, Jan. 2009.

[8] M. Luisier and A. Schenk, “Atomistic simulation of nanowire transistors,” *J. Comput. Theor. Nanosci.*, vol. 5, no. 6, pp. 1031–1045, Jun. 2008.

[9] A. Rahman, J. Guo, S. Datta, and M. S. Lundstrom, “Theory of ballistic nanotransistors,” *IEEE Trans. Electron Devices*, vol. 50, no. 9, pp. 1853–1864, Sep. 2003.

[10] A. Paul, M. Luisier, N. Neophytou, R. Kim, M. McLennan, M. Lundstrom, and G. Klimeck, Band Structure Lab, 2006, DOI: 10254/nanohub-r1308.12. [Online]. Available: https://www.nanohub.org/tools/bandstrlab

[11] A. Paul, S. Mehrotra, M. Luisier, and G. Klimeck, “On the validity of the top of the barrier quantum transport model for ballistic nanowire MOSFETs,” in *Proc. 13th Int. Workshop Comput. Electron.*, May 2009, pp. 1–4.

[12] M. Shin, "Full-quantum simulation of hole transport and band-to-band tunneling in nanowires using the $k \cdot p$ method," *J. Appl. Phys.*, vol. 106, no. 5, pp. 054 505-1–054 505-10, 2009.
[13] M. Shin, KP Nanowire/UTB FET, 2009, DOI: 10254/nanohub-r6510.2. [Online]. Available: https://www.nanohub.org/tools/kpnanofet
[14] E. Kane, "Energy band structure in p-type germanium and silicon," *J. Phys. Chem. Solids*, vol. 1, no. 1/2, pp. 82–99, 1956.
[15] P. Enders and M. Woerner, "Eight-band $k \cdot p$ Hamilton matrix for strained tetrahedral semiconductors : 4×4 block diagonalization for symmetric k-directions," *Phys. Stat. Sol. (B)*, vol. 194, no. 2, pp. 585–599, 1996.
[16] M. El kurdi, G. Fishman, S. Sauvage, and P. Boucaud, "Comparison between 6-band and 14-band $k \cdot p$ formalisms in SiGe/Si heterostructures," *Phys. Rev. B, Condens. Matter*, vol. 68, no. 16, pp. 165 333-1–165 333-16, 2003.
[17] S. Kim, M. Luisier, B. P. Haley, A. Paul, S. R. Mehrotra, and G. Klimeck, OMEN Nanowire, 2008, DOI: 10254/nanohub-r5359.6. [Online]. Available: https://www.nanohub.org/tools/omenwire
[18] R. Enderlein and N. J. M. Horing, *Fundamentals of Semiconductor Physics and Devices*. Singapore: World Scientific, 1997.
[19] J. Wang, E. Polizzi, and M. Lundstrom, "A three-dimensional quantum simulation of silicon nanowire transistors with the effective-mass approximation," *J. Appl. Phys.*, vol. 96, no. 4, pp. 2192–2203, Aug. 2004.
[20] M. Shin, "Computational Study on the performance of multiple-gate nanowire Schottky-Barrier MOSFETs," *IEEE Trans. Electron Devices*, vol. 55, no. 3, pp. 737–742, Mar. 2008.
[21] M. Shin, "Efficient simulation of silicon nanowire field effect transistors and their scaling behavior," *J. Appl. Phys.*, vol. 101, no. 2, pp. 024 510-1–024 510-6, 2007.

Mincheol Shin was born in Hong Sung, Korea, in 1965. He received the B.S. degree in physics from Seoul National University, Seoul, Korea, in 1988 and the Ph.D. degree in physics from Northwestern University, Evanston, IL, in 1992.

From 1993 to 2002, he was a Senior Researcher with the Basic Research Department, Electronics and Telecommunications Research Institute, Daejeon, Korea. In 2002, he joined the faculty of the School of Engineering, Information and Communications University, Daejeon. In 2009, the university was merged with Korea Advanced Institute of Science and Technology, where he is currently an Associate Professor with the Department of Electrical Engineering. His research interests are the transport in quantum wires and quantum dots, single-electron tunneling phenomena, and other mesoscopic physics. His current research interests are quantum simulations of nanoscale semiconductor and molecular devices.

Sunhee Lee received the B.S. and M.S. degrees in electrical and computer engineering from Seoul National University, Seoul, Korea, in 1999 and 2001, respectively. He is currently working toward the Ph.D. degree with the Network for Computational Nanotechnology, School of Electrical and Computer Engineering, Purdue University, West Lafayette, IN.

From 2001 to 2006, he was a Research Engineer with the Telecommunication Division, Samsung Electronics. He is working on the development of the nanoelectronic modeling tool NEMO 3-D, which is a self-consistent quantum mechanical tool that enables the simulation of multimillion-atom quantum-dot systems. His current research interests include identifying the band-structure properties of III–V devices, computational modeling of quantum-mechanical transport, and exploring electronic properties of ultradense impurity systems.

Gerhard Klimeck received the German Electrical Engineering degree from Ruhr-University Bochum, Bochum, Germany, in 1990 and the Ph.D. degree from Purdue University, West Lafayette, IN, in 1994.

He is currently with the School of Electrical and Computer Engineering, Purdue University, where he is the Director of the Network for Computational Nanotechnology and a Professor of electrical and computer engineering. He leads the development and deployment of web-based simulation tools, research seminars, tutorials, and classes that are hosted on http://nanohub.org, which is a community website that is utilized by over 120 000 users annually. He was the Technical Group Supervisor for the Applied Cluster Computing Technologies Group and continues to hold his appointment as a Principal Member at the NASA Jet Propulsion Laboratory on a faculty part-time basis. Previously, he was a Member of Technical Staff with the Central Research Laboratory of Texas Instruments. He has been the lead on the development of NEMO 3-D, which is a tool that enables the simulation of tens-of-million-atom quantum-dot systems, and NEMO 1-D, which is the first nanoelectronic computer-aided-design tool. His work is documented in more than 250 peer-reviewed publications and more than 400 conference presentations. His research interest is the modeling of nanoelectronic devices, parallel cluster computing, and genetic algorithms.

Dr. Klimeck is a member of the American Physical Society, Eta Kappa Nu, and Tau Beta Pi.